

High-Resolution Crystal Structures and Spectroscopy of Native and Compound I Cytochrome *c* Peroxidase[†]

Christopher A. Bonagura,^{*,§,||} B. Bhaskar,^{‡,§} Hideaki Shimizu,^{‡,⊥} Huiying Li,[‡] M. Sundaramoorthy,[@]
Duncan E. McRee,[#] David B. Goodin,⁺ and Thomas L. Poulos^{*,‡}

Program in Macromolecular Structure, Department of Molecular Biology and Biochemistry, University of California, Irvine, California 92697-3900, Departments of Medicine and Nephrology and of Biochemistry, Vanderbilt University Medical Center, Nashville, Tennessee 37232-2372, Syrrx, Inc., 10410 Science Center Drive, San Diego, California 92121, and The Scripps Research Institute, 10550 North Torrey Pines Road, La Jolla, California 92037

Received January 13, 2003; Revised Manuscript Received February 27, 2003

ABSTRACT: Cytochrome *c* peroxidase (CCP) is a 32.5 kDa mitochondrial intermembrane space heme peroxidase from *Saccharomyces cerevisiae* that reduces H₂O₂ to 2H₂O by oxidizing two molecules of cytochrome *c* (cyt *c*). Here we compare the 1.2 Å native structure (CCP) with the 1.3 Å structure of its stable oxidized reaction intermediate, Compound I (CCP1). In addition, crystals were analyzed by UV–vis absorption and electron paramagnetic resonance spectroscopies before and after data collection to determine the state of the Fe(IV) center and the cationic Trp191 radical formed in Compound I. The results show that X-ray exposure does not lead to reduction of Fe(IV) and only partial reduction of the Trp radical. A comparison of the two structures reveals subtle but important conformational changes that aid in the stabilization of the Trp191 cationic radical in Compound I. The higher-resolution data also enable a more accurate determination of changes in heme parameters. Most importantly, when one goes from resting state Fe(III) to Compound I, the His–Fe bond distance increases, the iron moves into the porphyrin plane leading to shorter pyrrole N–Fe bonds, and the Fe(IV)–O bond distance is 1.87 Å, suggesting a single Fe(IV)–O bond and not the generally accepted double bond.

Peroxidases are single-chain heme-containing enzymes ranging in mass from 30 000 to 40 000 Da. Traditional peroxidases catalyze the following multistep reactions (1).



In step 1, the peroxide O–O bond is broken, giving water, and a second peroxide-derived oxygen atom remains coordinated to the iron. The iron-linked oxygen formally contains only six valence electrons and is, therefore, a potent oxidizing agent (2). One electron is removed from the iron to give the oxy–ferryl intermediate [Fe(IV)–O], and a second electron

is removed from the porphyrin (P in the above scheme) to give a porphyrin π -cation radical (3).

Cytochrome *c* peroxidase (CCP)¹ is found in the mitochondrial intermembrane space of *Saccharomyces cerevisiae* where it catalyzes the reduction of peroxide to water. In CCP, a tryptophan side chain and not the porphyrin is oxidized to a cationic radical (4–6). In steps 2 and 3, Compound I is reduced in two successive one-electron transfer reactions back to the resting native state. Most well-studied peroxidases oxidize a variety of organic phenols and dyes, while CCP is highly specialized to oxidize ferrocycytochrome *c* (7).

Compounds I and II are easily distinguished by their different colors and spectral properties. The formation of such spectroscopically distinct intermediates has considerable historical significance since much of the early development of enzyme rapid reaction kinetics methods was developed in the 1940s using peroxidases (8). The Fe(IV) center also is thought to play an important role in cytochrome P450s (2), nitric oxide synthase, and cytochrome *c* oxidase (9). Although attempts have been made to structurally characterize the Fe(IV) intermediate in P450s (10), it now is clear that the P450 Fe(IV) intermediate is a transient species (11) whose existence can only be inferred. Peroxidases remain the prime targets for such structural characterizations primarily because the relative stability of Compounds I and II

[†] This research was supported in part by National Institutes of Health Grants GM42614 (T.L.P.) and GM41049 (D.B.G.).

* To whom correspondence should be addressed. E-mail: poulos@uci.edu. Telephone: (949) 824-7020. Fax: (949) 824-3280.

[‡] University of California.

[§] These authors contributed equally to this work.

^{||} Current address: Exelixis, Inc., 170 Harbor Way, So. San Francisco, CA 94083-0511.

[⊥] Current address: Molecular Neuropathology Group, RIKEN Brain Science Institute, 2-1 Hirosawa, Wako-shi, Saitama 351-0198, Japan.

[@] Vanderbilt University Medical Center.

[#] Syrrx, Inc.

⁺ The Scripps Research Institute.

¹ Abbreviations: CCP, cytochrome *c* peroxidase; cyt *c*, cytochrome *c*; HRP, horseradish peroxidase; MPD, 2-methyl-2,4-pentanediol; EPR, electron paramagnetic resonance; PDL, protein dipole Langevin dipole; EXAFS, extended X-ray absorption fine structure.

has made it possible to use a variety of biophysical probes to study the structure and spectroscopic properties of these intermediates (1). Such probes include X-ray crystallography, and to date, peroxidases remain the only enzyme system where an Fe(IV) intermediate has been trapped in the crystalline state and the structure determined. The solution of the CCP Compound I structure determined to 2.5 Å resolution represented the first such structure (12). This *tour de force* study required the merging of several data sets from different crystals since it was possible to collect only ~4 h worth of X-ray data because of the decay of Compound I at the temperature used for data collection, -15 °C. With the advent of Laue methods for rapid data collection, the structure of CCP Compound I was determined to 2.2 Å (13). However, the data were only 42.5% complete between 11.8 and 2.2 Å. These studies clearly showed that the Fe atom moves away from the proximal His ligand into the porphyrin core and the presence of the O atom linked to the iron. However, the determination of precise bond distances, geometry, and minor, but important, conformational changes was not possible because of the limited resolution and/or completeness of the data sets.

It has become increasingly clear that an important problem with such studies is the uncertainty of the redox state of the metal center and radical state in the X-ray beam. X-rays generate potent reducing equivalents in the form of hydrated electrons (10). Since Compound I is a strong oxidizing agent, it is possible that Fe(IV) and the radical center in Compound I will be reduced during data collection. This problem was recognized by Jouve et al. (14), who coupled crystallography and single-crystal microspectrophotometry to determine the crystal structure of catalase Compound I. In effect, the determined bond lengths in earlier studies might be an average of several states of the protein because of the experimental exposure to X-rays at higher temperatures. However, we reasoned since CCP Compound I is indefinitely stable at cryogenic temperatures, it should be possible to freeze Compound I in the crystalline state and then use more traditional data collection methods at a modern synchrotron source, rather than the more complex Laue method. With the routine use of cryogenic data collection coupled with the new generation of synchrotron X-ray sources, we have found that crystals of CCP will, on occasion, diffract to near-atomic resolution. This has provided an opportunity to obtain data from crystals of resting state CCP and Compound I to 1.2 and 1.3 Å, respectively. In addition, UV-vis and single-crystal electron paramagnetic resonance spectroscopy have been utilized to characterize the state of the crystals before and after X-ray exposure during data collection. This paper describes these results and their implications on the reaction mechanism.

MATERIALS AND METHODS

Crystal Growth and Compound I Formation. CCP used in this study was purified from an *Escherichia coli* expression system (15). CCP diffraction quality crystals were grown using standard conditions of 300 μM protein mixed 1:1 with mother liquor containing 50 mM potassium phosphate (pH 6.0) and 30% 2-methyl-2,4-pentanediol (MPD) according to the method of Edwards and Poulos (16) as later modified by Sundaramoorthy et al. (17). Sitting drops (20 μL) set in siliconized nine-well glass plates were touch-seeded and

incubated at 4 °C for ~4 days. The best crystals of smaller dimensions, approximately 200 μm on the longest edge, were chosen to ensure low mosaicity.

Compound I was formed in the crystal by soaking similar CCP crystals in mother liquor [35% MPD and 50 mM Tris-phosphate (pH 6.0)] containing 10 mM hydrogen peroxide for 1 h followed by soaking in 35% MPD in 50 mM Tris-phosphate (pH 6.0) to remove excess peroxide. Several similar crystals were treated in this fashion to form Compound I. One of those crystals was dissolved in 50 μL of 50 mM potassium phosphate (pH 6.0), and the spectrum was measured using a 50 μL microcuvette in an HP 8452A diode array spectrophotometer equipped with UV-vis Chemstation (version 02.05) software. Another Compound I crystal was used for X-ray data collection, and after the experiment, the X-ray-exposed crystal was again dissolved in 50 μL of 50 mM potassium phosphate (pH 6.0) and the spectrum measured using the same 50 μL microcuvette. Despite the high concentrations of peroxide that were used, the refined electron density maps showed no indication of damage to residues susceptible to peroxide oxidation such as Trp, Tyr, and Met.

X-ray Data Collection, Indexing, and Data Reduction. All data were collected at cryogenic temperatures in a stream of liquid nitrogen. Since CCP crystals are grown from solutions containing MPD, there was no need for the addition of cryosolvents. Synchrotron X-ray data were obtained by two separate scans at low and high resolution at SSRL beamline 9-1 on a MAR345 imaging plate system with 0.78 Å incident X-ray light. In-house data were obtained using an R-AXIS IV imaging plate system and a Rigaku RU-300 copper rotating anode generator equipped with Osmic optics. A single crystal was utilized for each data set. Data were processed with DENZO (18) or MOSFLM (19) and scaled with SCALEPACK (18). Data were subsequently reduced again using DPS-MOSFLM (19) to verify statistics independently (data not shown), and the model that was used was further refined against this independently reduced data showing an overall improvement in *R*-factors.

Refinement initially was carried out using CNS (version 1.1) (20) and in the later stages SHELXL (21). For the resting enzyme, refinement was initiated in SHELXL at 1.7 Å and moved progressively to higher resolution until at cycle 7 all data to 1.20 Å were included. We began by using rigid body refinement as implemented in CNS, followed by simulated annealing and the calculation of a composite omit map to begin model building. After each cycle of refinement, solvent molecules selected automatically using an $F_o - F_c$ difference map cutoff of 4.0σ were visually examined. Those with a high temperature factor, usually ≥ 60 , were eliminated. Much care was taken in modeling the solvent in these structures as even tertiary shell water molecules were apparent and had to be addressed using partial occupancy. Many routines for automating water picking were attempted, such as CNS, ARP/WARP, or SHELXL, finally settling on the SHELXL water picking capabilities. The inclusion of anisotropic *B*-factors toward the end of refinement was justified on the basis of a drop in R_{free} . The N-Fe and O-Fe distances were not restrained during refinement. The same strategy was used for refinement of Compound I using an early stage native structure through simulated annealing before beginning

Table 1: X-ray Data Collection and Refinement Statistics

	native synchrotron	Compound I synchrotron	native in-house	Compound I in-house
unit cell				
space group	$P2_12_12_1$	$P2_12_12_1$	$P2_12_12_1$	$P2_12_12_1$
cell parameters (Å)	$a = 106.67$ $b = 75.51$ $c = 50.94$	$a = 106.81$ $b = 74.81$ $c = 50.92$	$a = 106.628$ $b = 75.080$ $c = 50.931$	$a = 107.203$ $b = 75.7271$ $c = 51.098$
data collection				
resolution range (Å)	100.0–1.20	100.0–1.29	100.0–1.75	100.0–1.80
total no. of observations	1275193	1157938	479863	623690
no. of independent reflections	126775	102834	40567	38501
completeness (all data) (%)	96.80	93.60	96.20	97.70
$R_{\text{sym}}(I)^a$	0.071	0.048	0.048	0.066
$I/\sigma(I)$	12.20	12.90	36.42	25.12
last shell resolution (Å)	1.22–1.20	1.31–1.29	1.78–1.75	1.83–1.80
completeness (%)	74.0	55.1	71.40	95.80
$R_{\text{sym}}(I)^a$	0.437	0.331	0.347	0.539
$I/\sigma(I)$	1.99	1.97	3.34	1.975
refinement				
resolution range (Å)	10.0–1.20	10.0–1.29	50.0–175	50.0–1.80
no. of reflections (σI cutoff = 0)	120831	91721	39634	36942
R_{free} (% set aside)	0.1506 (2.6%)	0.1552 (4.0%)	0.1980 (4.8%)	0.2042 (4.7%)
R_{cryst}^b	0.1143	0.1162	0.1753	0.1794
rms deviation ^c				
bond lengths (Å)	0.016	0.014	0.0049	0.049
angle distances	0.029	0.029	2.25	2.28
no. of fully occupied water molecules (partially occupied)	622 (196)	522 (102)	485 (2)	463

^a $R_{\text{sym}} = \sum |I_h - I_h| / \sum I_h$. ^b $R_{\text{cryst}} = \sum (|F_{\text{obs}}| - |F_{\text{calc}}|) / \sum |F_{\text{obs}}|$. ^c The rmsd for bond lengths and the rmsd for angle distances represent the root-mean-square deviations between the observed and ideal values.

refinement against the new data. A summary of data collection and refinement is provided in Table 1.

Standard uncertainties in bond lengths were calculated by inversion of the normal matrix using SHELXL. All restraints on positional parameters were excluded for the calculation. The matrix included all of the positional parameters and none of the thermal parameters. Previous work with standard uncertainty calculations on other protein systems had shown that this inclusion of the thermal parameters results in a <1% difference in the values calculated for bond length errors.

Electron Paramagnetic Resonance Spectroscopy. Single-crystal EPR spectra were collected by mounting crystals on nylon loops attached to X-ray goniometer pins constructed from Kel-F. After being frozen, the crystal and pin assembly could be transferred to the bottom of a 4 mm quartz tube and glued in place with 50% methanol, allowing insertion into a standard cryostat of an X-band microwave cavity. The transfer was accomplished under liquid N₂ so that crystals could be moved from the diffractometer to the EPR cavity and back without thawing. EPR spectra were collected as a function of the tube rotation axis, allowing the signal anisotropy to be evaluated. In cases where the same crystal was examined before and after X-ray exposure, orientations were selected that gave a similar line shape, allowing more facile comparison of signal amplitudes. EPR spectra in this work were collected at 9 K using a microwave power of 10 mW and a field modulation of 10 G at 100 kHz. When necessary, a background spectrum collected without the crystal was subtracted from the data.

Computational Methods. The relative electrostatic stability of the Trp191 cationic radical was analyzed using the protein dipoles Langevin dipole (PDL) method (22) as implemented in the MOLARIS package of programs (version 9.06, <http://laetro.usc.edu/programs/index.html>). The procedures

closely followed the work of Jensen et al. (23). The PDL method divides the protein and solvent into four regions. Region I consists of the indole atoms of Trp191. Region II is defined by the surrounding protein at a radius r_1 from the center of region I. Region III consists of the Langevin dipole grid of radius r_2 centered on region I. Solvent is modeled as Langevin dipoles fixed on the grid but free to reorient. The system beyond region III, region IV, is modeled as a continuum dielectric with a dielectric constant of 80. The various radii were the default values provided in the program package. Charges for the cationic Trp191 indole ring were taken from Jensen et al. (23) and are based on a density functional calculation using a Becke3LYP functional and 6-31G* basis set. Asp235, which H-bonds with Trp191 and the proximal His175 heme ligand, was given a net charge of -1.0 . The $\Delta\Delta G$ values reported here are based on static X-ray structures.

RESULTS

Spectroscopy. The simplest method for checking the state of the Fe(IV)–O center before and after exposure to X-rays is UV–vis absorption spectroscopy. However, the main Soret band has a large extinction coefficient which precludes the use of the single-crystal microspectrophotometer available to us since too much light is absorbed by the relatively thick crystals used in these studies. We therefore washed Compound I crystals in peroxide-free mother liquor followed by dissolving the crystal in peroxide-free buffer. The solution spectrum of the dissolved crystal was recorded before and after data collection for crystals treated with and without peroxide (Figure 1A). The resting state crystal before and after X-ray exposure exhibited the characteristic spectrum of high-spin ferric CCP with a broad Soret absorption maximum of 408 nm, showing that X-rays do not affect the

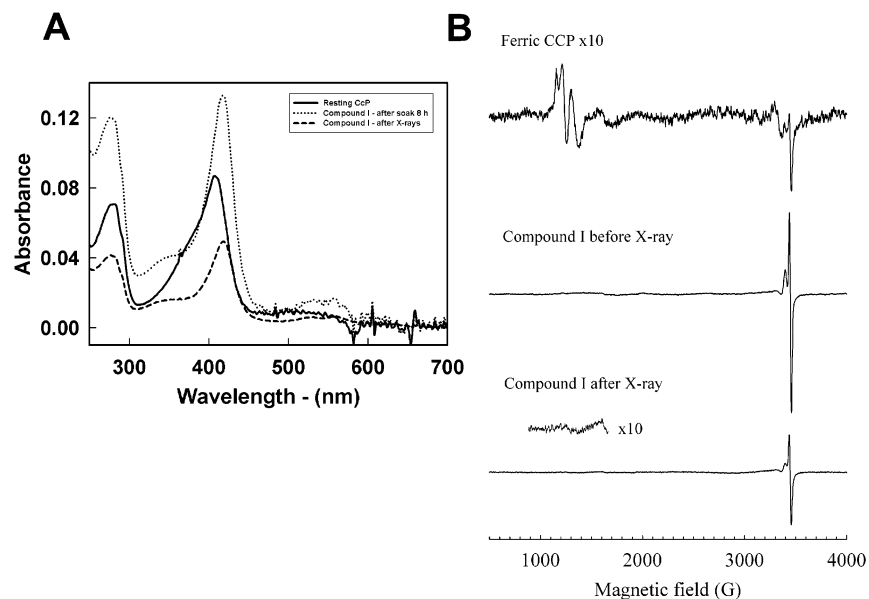


FIGURE 1: (A) Absorption spectra of crystals dissolved in buffer. Crystals treated with peroxide were first washed in peroxide-free mother liquor and then dissolved in peroxide-free buffer. A different crystal was used for each spectrum. (B) EPR spectra collected at 9 K of single crystals of CCP. The top spectrum was obtained from a crystal of native CCP oriented to show ferric heme signals near $g = 6$. A crystal of CCP in the Compound I state is shown before exposure to X-rays in the central spectrum and after structure determination (X-ray exposure for 12 h on a rotating anode X-ray source) in the bottom spectrum. Approximately 50% of the Trp191 radical remains after exposure, and no evidence of ferric heme is observed.

Fe(III) center. The spectrum of the peroxide-treated crystal before and after exposure to X-rays remained unchanged as evidenced by the retention of the Soret absorption maximum at 420 nm and the presence of α/β bands at 530 and 560 nm. These results were consistently reproduced with several crystals and show that the Fe(IV)–O center is not reduced in the X-ray beam.

A separate determination of the oxidation state of these crystals was obtained by low-temperature single-crystal EPR. The spectrum of a native crystal is shown in Figure 1B and displays signals near $g = 6$, reflecting the high-spin ferric heme. At least three signals are seen in this spectrum, arising from the different orientations of the four molecules in the unit cell. Also shown in Figure 1B is a crystal of CCP Compound I, prepared in a manner identical to that used for structure determination. The complete loss of the ferric signals is consistent with conversion to the Fe(IV) oxidation state, and the appearance of the intense asymmetric signal near $g = 2$ is characteristic of the Trp191 radical of Compound I. The effects of X-ray exposure on this crystal were examined by transferring it to a goniometer where it was exposed for 12 h to Cu $K\alpha$ radiation from a rotating anode generator. After X-ray data collection, the crystal was returned to the EPR cryostat and its EPR signal recorded. The EPR spectrum in Figure 1B after X-ray exposure shows that the intensity of the Trp191 radical is diminished to ~50% of that of the original sample, indicating that the radical state has been partially reduced by X-ray exposure, time, or handling. However, no evidence is seen for return of the ferric signals. These data, when combined with the UV–vis spectra, indicate that the heme center remains in the Fe(IV) ferryl state during data collection.

Disorder. The overall structure of CCP is shown in Figure 2 together with key regions relevant to this study highlighted. The major new insights into CCP function derived from these higher-resolution structures stem from those regions of the

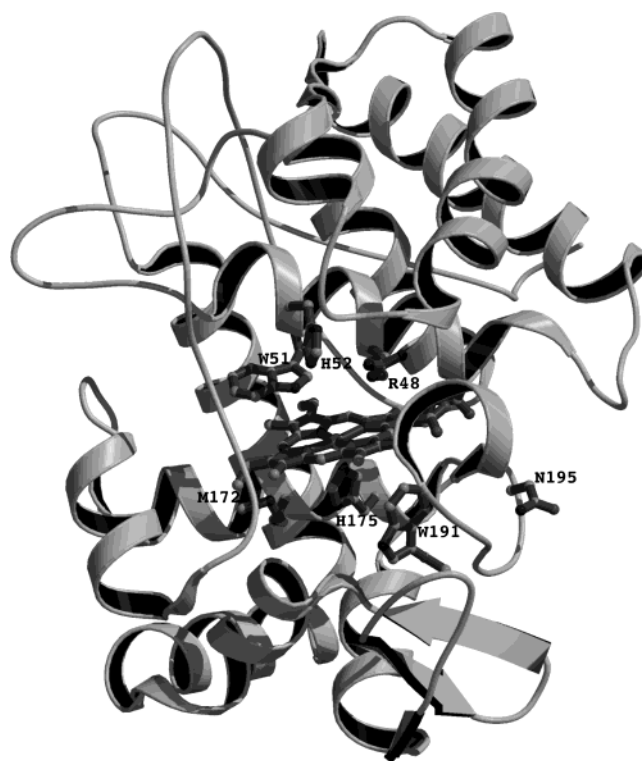


FIGURE 2: CCP molecule highlighting key regions of the structure relevant to this study.

structure where differences are seen in discrete disorder between the resting and Compound I states.

There are three such regions, and in all three, the protein is more ordered in Compound I. The first of these is Arg48 in the distal pocket which is considered to be a key residue involved in the formation of Compound I (24, 25). In resting state CCP, Arg48 occupies two positions, one “out” toward the heme propionate and the other “in” toward the heme iron (Figure 3). In Compound I, Arg48 occurs in the “in” position

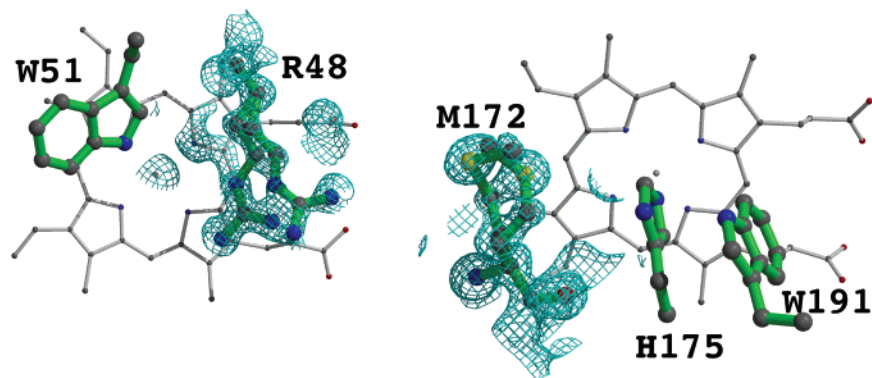
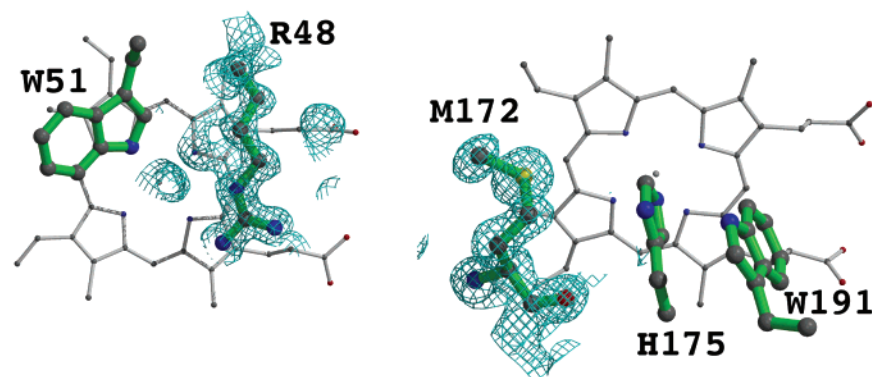
Resting state 2Fo-Fc at 2 σ **Compound I 2Fo-Fc at 2 σ** 

FIGURE 3: Sections of the $2F_o - F_c$ electron density maps for the resting state and CCP Compound I. Arg48 and Met172 occupy two positions in the resting state but only one in Compound I.

which enables Arg48 to H-bond with the ferryl O ligand (Figure 4). The “in” position has been observed in earlier structures of CCP Compound I (12, 13) and in the CCP–fluoride complex (26). A second residue that becomes more ordered in Compound I is Met172 in the proximal pocket. In the resting state, this residue is best modeled in two conformations (Figure 3). In Compound I, Met172 occupies the position closer to the proximal His175 ligand (Figure 3). The distance between the Met172 SG atom and His175 varies from 6.4 Å in the resting state position furthest from the His ligand to 4.4 Å in Compound I.

Residues 193–195, including both side chains and peptide backbone, constitute the third and last region that becomes more ordered in Compound I (Figure 5). Ala194 and Asn195 adopt multiple conformations in the resting state, but only one of these is observed in Compound I. The single conformation observed in Compound I is shown in Figure 6. In this conformation, the side chain of Asn195 is in position to donate an H-bond to the peptide carbonyl oxygen of Gly178. Gly178, in turn, is 4.01 Å from Trp191. The Asn195–Gly178 H-bond thus helps to stabilize a section of polypeptide in direct contact with the Trp191 cation radical. In addition to helping stabilize the positive charge on the Trp191 radical, Asn195 also sits at the interface in the crystal structure of the CCP–cyt *c* non-covalent complex (27).

Since we are correlating the spectroscopy with crystal structures and the spectral results were obtained with crystals exposed on an in-house X-ray source, it is important to compare the models derived from in-house data with synchrotron data. The native structure using in-house data

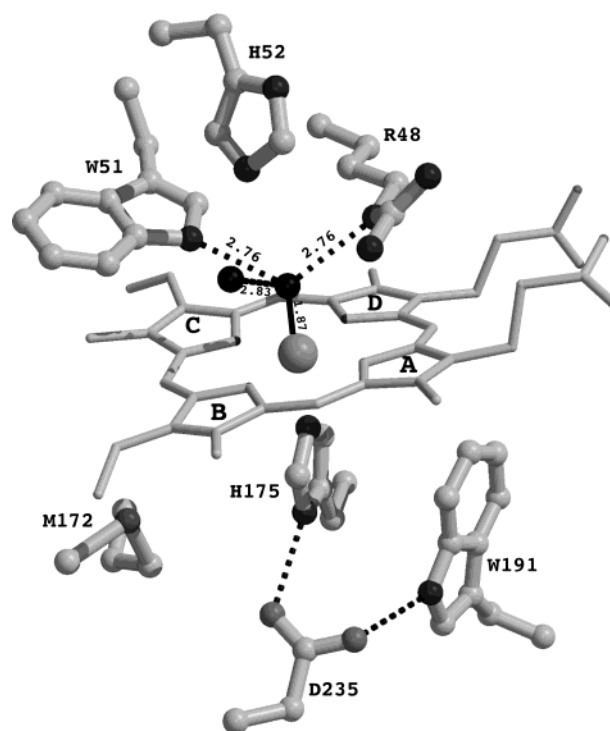


FIGURE 4: H-Bonding pattern and distances in the distal pocket in Compound I. The distances are in angstroms.

also exhibited disorder, while in-house Compound I data sets did not, exactly as in the synchrotron-derived structures. However, the lower resolution of the in-house data sets, 1.7–

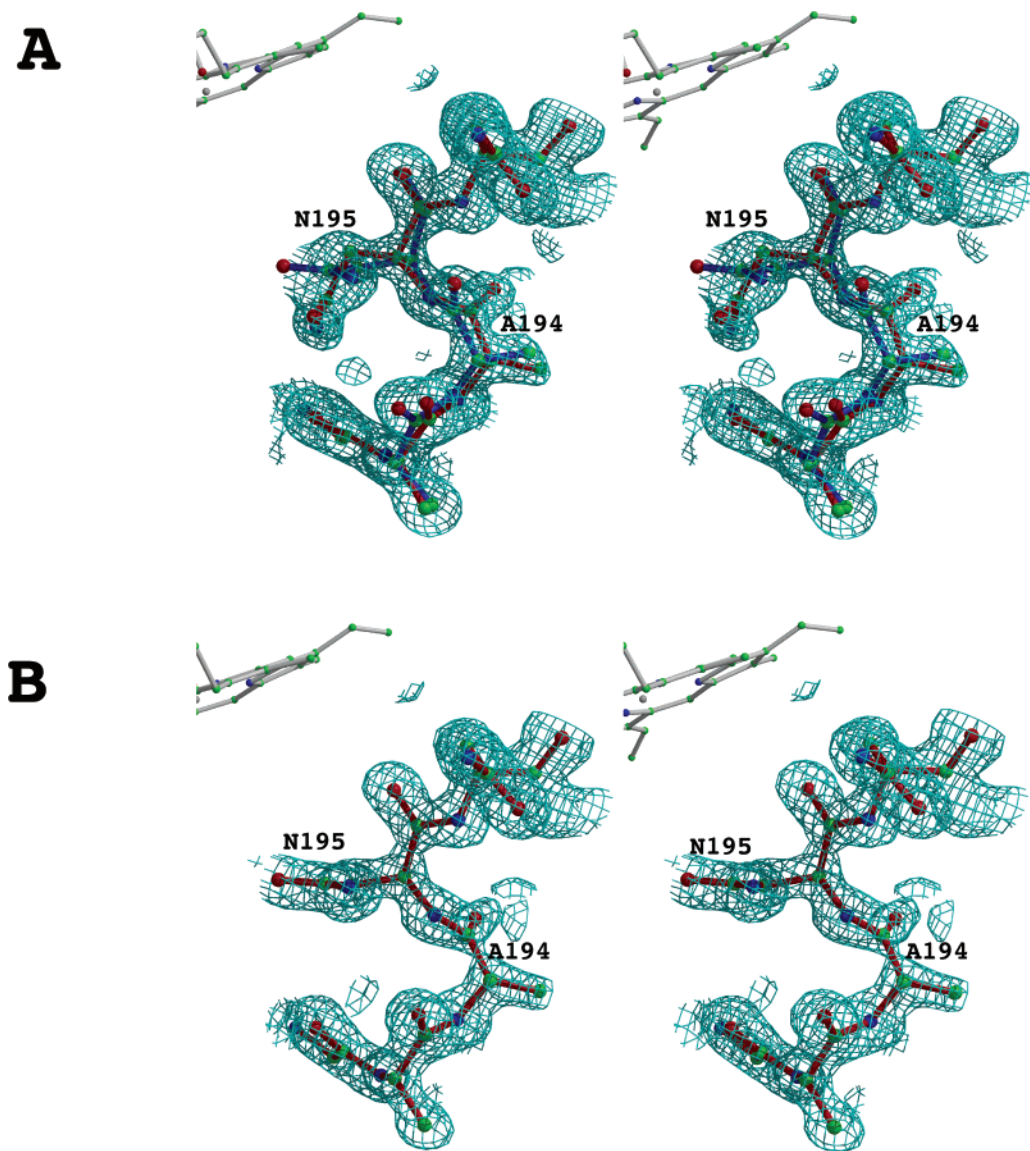


FIGURE 5: Stereoviews of the $2F_o - F_c$ electron density maps centered on Asn195 contoured at 2.0σ . In the resting state (A), this segment of the molecule exhibits two conformations, while only one conformation is present in Compound I (B).

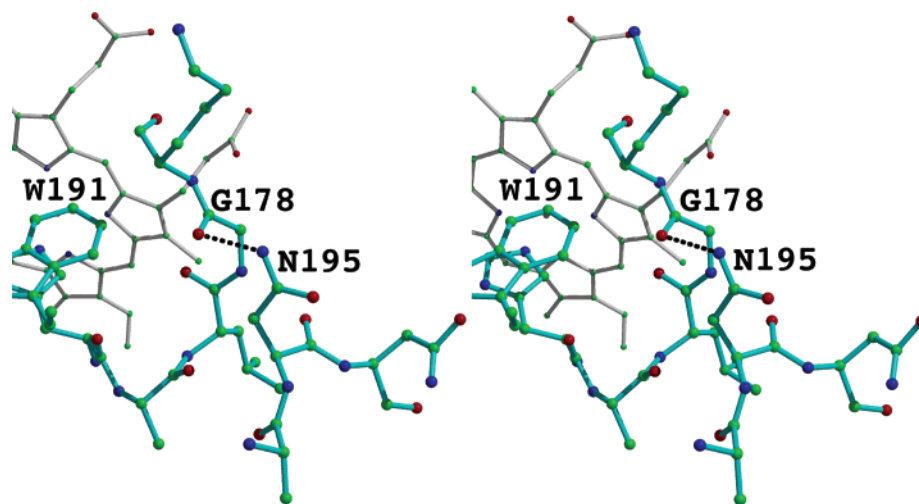


FIGURE 6: Stereodiagram showing the Asn195 region in Compound I. In this conformation, Asn195 H-bonds with a section of polypeptide that directly contacts the Trp191 cation radical, thus providing additional stability to the positively charged radical.

1.8 Å, precluded an accurate modeling of multiple conformations. For example, the region of residues 193–196 appears as weak electron density with high thermal factors, and the

$F_o - F_c$ maps were simply not clear enough to accurately model multiple conformations. In addition, the in-house Compound I data sets exhibited much cleaner electron

Table 2: Results of Electrostatic Calculations Using MOLARIS^a

protein	$\Delta\Delta G(\text{water} \rightarrow \text{protein})$ (kcal/mol, dielectric = 4)
Compound I with Met172, "out" conformation ^b	-6.16
Compound I with Met172, "in" conformation	-7.22
native residues 193-195, "out" conformation	-5.87
native residues 193-195, "in" conformation	-6.16

^a The more negative the $\Delta\Delta G$ value, the more stable the Trp191 cationic radical. ^b The "out" conformations are one of two observed in the native structure and are observed only in the native structure. The "in" conformations represent the single conformations observed in Compound I.

density for residues 193-196 and the Fe(IV)-O center was clearly defined. The excellent correlation between in-house and synchrotron data sets justifies using crystals exposed to in-house X-ray sources for the spectroscopic studies.

To gain further insights into the role such conformational differences might play in stabilizing the Trp191 radical, the PDL computational method (22), which has been successfully used in CCP (23), was employed. The basic property to be compared is the $\Delta\Delta G$ of transferring the Trp191 cationic radical from solvent to protein. Although this is not a physically "real" process, this method provides a basis for comparing the electrostatic stabilization of the Trp191 cationic radical in various protein environments. This procedure predicted that the Trp191 cationic radical is more stable in CCP than in the homologous ascorbate peroxidase (23) which agrees with the experimental results (28, 29). In our case, four POLARIS calculations were carried out (Table 2) and were designed to address the question of how much the conformational mobility of Met172 and residues 193-195 contributes to the electrostatic stabilization of the Trp191 cationic radical. The various conformations are designated "in" and "out". The "out" conformations of Met172 and residues 193-195 are unique to the native structure, while the "in" conformations are the single conformations observed in Compound I. As shown in Table 2, the Trp191 cationic radical is most stable in Compound I using the "in" conformation of Met172 as seen in the crystal structure of Compound I. When Met172 was modeled in the Compound I structure in the "out" position, one of the two conformers seen in the native structure, the Trp191 cationic radical is less stable. This seems reasonable since the in position of Met172 places the side chain S atom closer to Trp191 and, hence, the electronegative S atom can more effectively aid in stabilizing the charged radical. Table 2 further shows that the "out" conformation of residues 193-195 is less stabilizing than the Compound I in conformation. Therefore, it appears that the ordering of Met172 and residues 193-195 observed in Compound I contributes to the electrostatic stabilization of the Trp191 cationic radical.

Changes in Heme Geometry. To obtain an objective estimate of the various heme parameters, none of the Fe to ligand distances were restrained during refinement. Heme to ligand distances for the resting state and Compound I are provided in Table 3, and Figure 7 shows the electron density around the heme. When one goes from the resting state to Compound I, the His-Fe bond distance increases from 2.07 to 2.10 Å while the average pyrrole ring N-Fe distance decreases from 2.05 to 2.00 Å. These changes result from movement of the Fe atom into the porphyrin core by 0.24 Å

Table 3: Heme Parameters

	resting state	Compound I
Fe-His distance (Å)	2.07	2.10
Fe-pyrrole N distance (average) (Å)	2.05	2.00
Fe to pyrrole N plane (Å)	0.28	0.05
Fe(IV)-O distance (Å)	-	1.87
pyrrole N plane to porphyrin plane (deg)	2.86	1.65
pyrrole A plane to porphyrin plane (deg)	2.66	4.46
pyrrole B plane to porphyrin plane (deg)	5.74	4.92
pyrrole C plane to porphyrin plane (deg)	5.81	6.67
pyrrole D plane to porphyrin plane (deg)	8.85	7.12

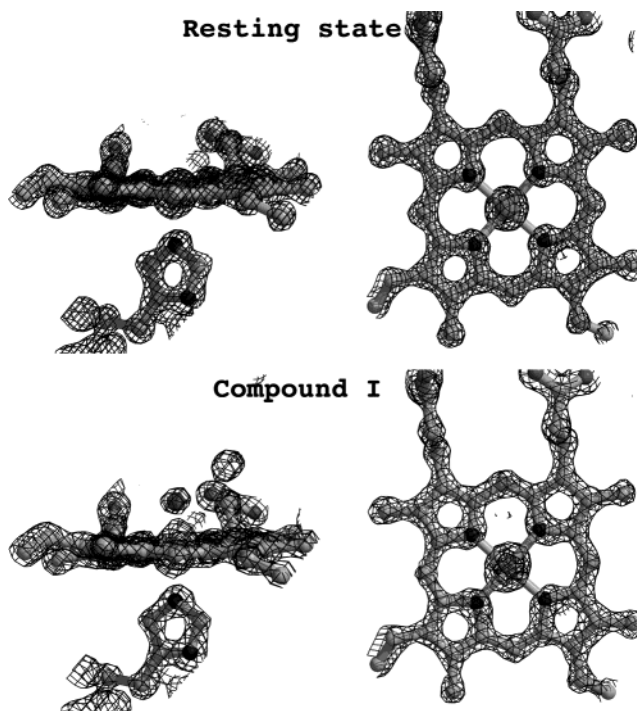


FIGURE 7: Electron density maps ($2F_o - F_c$) around the heme group in the resting state and Compound I. Both maps are contoured at 2.5σ .

which lengthens the His-Fe bond but shortens the pyrrole N-Fe bonds. There is a slight change, 0.14 Å, in the position of pyrrole rings A and D such that the plane formed by pyrrole ring N atoms lies closer to the overall heme plane. This motion is most likely due to Arg48 being locked in the "in" conformation which positions the Arg48 guanidine group closer to pyrrole rings A and D. The motion of rings A and D away from Arg48 and toward the proximal pocket thus relieves unfavorably close contacts between Arg48 and the heme. The Fe-O distance is 1.87 ± 0.02 Å with the error estimated from inversion of the least-squares matrix using SHELXL. The unconstrained Fe-O distance in the 1.8 Å resolution structure refined using in-house data is 1.76 Å.

DISCUSSION

Stability of Compound I. It has become evident that exposure of metalloprotein crystals to X-rays often can lead to reduction of the metal center (10). This can be especially problematic for intermediates such as Compounds I and II where the redox potential of the ferryl center is approximately 1 V (30). Our spectroscopic results show that CCP Compound I is remarkably stable to X-ray exposure. The Fe(IV)-O center is not affected by X-ray exposure as

evidenced by both absorption and EPR spectroscopy. In addition, the single-crystal EPR data indicate that by the end of data collection, approximately 50% of the Trp191 cationic radical signal remains. It should be noted that crystals used for the spectroscopic studies were exposed to X-rays using an in-house X-ray system, while the high-resolution work used synchrotron radiation. Despite the large difference in energy and intensity, the Fe(IV)–O centers in models obtained from either in-house or synchrotron data were the same, although the distances derived from the higher-resolution synchrotron-derived structure are more accurate. Therefore, neither in-house nor synchrotron radiation had any effect on the Fe(IV)–O center.

Nature of the Fe(IV)–O Bond. One of the more important results from this study is that the Fe(IV)–O bond length is 1.87 Å, which is longer than expected. There have been two previous X-ray studies of CCP Compound I, albeit, at lower resolution. The first of these was carried out prior to the routine use of cryogenic data collection, required the merging of several data sets, and was limited to 2.5 Å resolution (12). The second study utilized Laue diffraction methods, and the resulting 2.2 Å structure gave an Fe(IV)–O distance ranging from 1.7 to 1.9 Å. The structures of catalase Compounds I and II have been determined using rapid Weissenberg data collection methods (14, 31), but the limited 2.7 Å resolution precludes accurate estimates of Fe(IV)–O bond distances. A recent study that closely parallels our current work is the 1.35 Å structure of myoglobin Compound II (32). In this case, the Fe(IV)–O bond distance was found to be 1.92 Å. The recent X-ray work on HRP Compounds I and II to 1.6 Å resolution gives Fe(IV)–O distances of 1.7 Å for Compound I and ~1.8 Å for Compound II (33). The heme of HRP Compound II and the heme of CCP Compound I are electronically equivalent, and hence, the longer Fe(IV)–O distance of 1.8 Å in HRP Compound II should be compared to the 1.87 Å distance in CCP Compound I.

These rather long Fe(IV)–O distances are at odds with some of the early EXAFS work on peroxidases. Chance et al. (34) estimated a distance of 1.67 Å in CCP Compound I, while Penner-Hahn et al. (35) estimated a distance of 1.6 Å for both Compounds I and II of HRP. However, Chance et al. (34) estimated an Fe(IV)–O distance of 1.93 Å in HRP Compound II and comes closest to agreeing with the 1.8 Å distance observed in the HRP Compound II crystal structure (33). Although the EXAFS results differ from the crystal structures, resonance Raman data more closely match the current X-ray results. Reczek et al. (36) found that the Fe(IV)–O stretch in CCP Compound I was 753 cm⁻¹ [although see ref 37, the authors of which assigned a 767 cm⁻¹ stretching frequency to the Fe(IV)–O center in CCP Compound I] compared to 773–779 cm⁻¹ for HRP (36–39), indicating a weaker Fe(IV)–O bond in CCP. Reczek et al. (36) argued that the lower frequency they observed for the Fe(IV)–O stretch in CCP Compound I was due to a strong H-bond to the Fe(IV)–O oxygen and greater single-bond character of the Fe(IV)–O bond. This is consistent with the structure in the work presented here since both Arg48 and Trp51 form H-bonds with the ferryl O atom and the long 1.87 Å Fe(IV)–O bond indicates a single bond. Mössbauer data for CCP Compound I also resemble those of a synthetic Fe(IV) porphyrin containing two methoxy oxygen ligands that form single bonds with the iron (40, 41).

Overall, the results presented here coupled with the weight of the spectroscopic data strongly favor a single Fe(IV)–O bond. A single bond also most certainly means that the ferryl O atom is protonated. Hersleth et al. (32) favor a description where a hydroxyl radical is coordinated to Fe(III). In peroxidases, we know that the peroxide O–O bond undergoes heterolytic cleavage (42) which leaves an O atom containing six valence electrons bound to the iron. In CCP, both Fe(III) and Trp191 are oxidized. If both electrons now reside primarily on the Fe-linked O atom, this O atom contains a full complement of eight valence electrons, giving an Fe(IV)–O⁻ center which should be a strong base and exist primarily as a Fe(IV)–OH center if the Fe(IV)–O bond is a single bond. The OH group is stabilized by strong H-bonding as predicted from the Raman studies (36) by motion of Arg48 as we have seen in the Compound I structure (Figure 4). Therefore, these data suggest that the ferryl center of CCP may best be described as a hydroxide ion with a single bond to Fe(IV) stabilized by H-bonding interactions with Arg48 and Trp51.

One remarkable feature of the ferryl intermediate in peroxidases is its stability. The distal Arg48 side chain contacts the ferryl O atom, yet the Arg is not oxidized. The crystal structure of a mutant of CCP where Arg48 is replaced with Ala shows that hydroxyguanidine binds in the active site to occupy the space of the missing Arg48 side chain (43). Here, too, neither guanidine nor arginine was oxidized by the mutant, although the more readily oxidized *N*-hydroxy derivatives were oxidized in a peroxide-dependent redox process (43). Very often, cytochrome P450s and nitric oxide synthase (NOS) are compared to peroxidases in having a highly reactive ferryl intermediate that rapidly hydroxylates a substrate. NOS provides an especially interesting comparison to peroxidases since the substrate, L-arginine, occupies a position in the active site very similar to that of the conserved arginine found in peroxidases (Arg48 in CCP). The crystal structure of the NO complex of the endothelial NOS heme domain (44) shows that the substrate directly H-bonds with the ligand. We would expect the hypothetical ferryl O atom in NOS to directly interact with the substrate guanidinium group, like what we see in CCP. However, in NOS the arginine is hydroxylated, while in CCP the arginine is very stable. Clearly, the Fe(IV)–O-like intermediates in NOS and P450 are very different from those in peroxidases which greatly limits the general homology drawn between these two classes of enzymes.

Disorder. The second major finding in this study is the ordering of two key regions upon formation of Compound I. Met172 occupies at least two positions in the resting state enzyme, one 6.4 Å and the second 4.4 Å from the proximal His175 ligand. In Compound I, only the shorter distance is observed. The second region involves residues 193–195 which are located at the closest point of contact between CCP and cyt *c* in the intermolecular electron transfer complex (27). The effect of residues 193–195 is less direct. In the resting enzyme, Asn195 occupies at least two orientations, but in Compound I, Asn195 is locked in a position where the side chain amide nitrogen H-bonds with the peptide carbonyl oxygen of Gly178 which, in turn, is 4.01 or 4.24 Å from Trp191. The electrostatic calculations support the view that the single conformations observed in Compound I aid in stabilizing the positive charge on the Trp191 cation

radical. Thus, there is a balance between the unfavorable loss of entropy in going from the disordered to the ordered state in forming Compound I which is balanced by the favorable enthalpic changes in stabilizing the Trp191 cation radical.

One potential paradox in correlating ordering of structural elements with the formation of the Trp191 radical is the fact that at the end of data collection, ~50% of the Trp191 EPR radical signal remains. If the Compound I data set represents a 50:50 mix of neutral and charged Trp191, then at 1.3 Å we should be able to see residual disorder in Met172 and residues 193–195. Yet it is quite clear that these regions occupy only one conformation in Compound I. There are two possible explanations. First, the ordering observed in Compound I is not just a consequence of forming the Trp191 radical but also a result of formation of the Fe(IV)–OH center. Second, the 50% loss in EPR signal could be an overestimate of how much signal is lost. For example, the kinetics of radical decay in the X-ray beam remain unknown. If most of the radical reduction occurs at later times, during sample preparation and handling, a majority of the data could constitute a fully oxidized Trp191 radical. In addition, the EPR data were obtained after exposure to Cu K α radiation using an in-house source. The shorter wavelength radiation used at the synchrotron is less effective at generating reducing equivalents (10), although this might be partially counterbalanced by the increase in intensity.

Despite these uncertainties, we hypothesize that the ordering of both regions in Compound I results from a tightening of the structure around the Trp191 cationic radical. In Compound I, Met172, His175, and Trp191 form a continuous π stacking interaction which can help stabilize the new positive charge on Trp191. Moreover, the Asn195 section of the polypeptide helps to stabilize a section of chain directly contacting Trp191. Our computational results further suggest that the conformation of Met172 and residues 193–195 observed in Compound I provides additional electrostatic stabilization to the cationic Trp191 radical.

On a somewhat more speculative note, an additional factor that may be important is that the Asn195 region directly contacts cyt *c* in the CCP–cyt *c* complex, and hence, the ordering of this region may assist in docking of the two redox partners and/or the electron transfer reaction.

REFERENCES

- Poulos, T. L., and Fenna, R. (1994) *Met. Biol.* 30, 25–75.
- Hamilton, G. (1974) in *Chemical models and mechanisms for oxygenases* (Hayaishi, O., Ed.) pp 405–451, Academic Press, New York.
- Dolphin, D., Forman, A., Borg, D. C., Fajer, J., and Felton, R. H. (1991) *Proc. Natl. Acad. Sci. U.S.A.* 68, 614–618.
- Sivaraja, M., Goodin, D. B., Smith, M., and Hoffman, B. M. (1989) *Science* 245, 738–740.
- Huyett, J. E., Doan, P. E., Gurbriel, R., Houseman, A. L. P., Sivaraja, M., Goodin, D. B., and Hoffman, B. M. (1995) *J. Am. Chem. Soc.* 117, 9033–9041.
- Houseman, A. L., Doan, P. E., Goodin, D. B., and Hoffman, B. M. (1993) *Biochemistry* 32, 4430–4443.
- Yonetani, T. (1976) in *The Enzymes* (Boyer, B., Ed.) pp 345–361, Academic Press, Orlando, FL.
- Chance, B. (1943) *J. Biol. Chem.* 151, 553–577.
- Witt, S. N., Blair, D. F., and Chan, S. I. (1986) *J. Biol. Chem.* 261, 8104–8107.
- Schlichting, I., Berendzen, J., Chu, K., Stock, A. M., Ringe, D., Petsko, G., and Sligar, S. G. (2000) *Science* 287, 1615–1622.
- Davydov, R., Makris, T. M., Kofman, V., Werst, D. E., Sligar, S. G., and Hoffman, B. M. (2001) *J. Am. Chem. Soc.* 123, 1403–1415.
- Edwards, S. L., Nguyen, H. X., Hamlin, R. C., and Kraut, J. (1987) *Biochemistry* 26, 1503–1511.
- Fulop, V., Phizackerley, R. P., Soltis, S. M., Clifton, I. J., Wakatsuki, S., Erman, J., Hajdu, J., and Edwards, S. L. (1994) *Structure* 2, 201–208.
- Jouve, H. M., Andreoletti, P., Gouet, P., Hajdu, J., and Gagnon, J. (1997) *Biochimie* 79, 667–671.
- Darwish, K., Li, H., and Poulos, T. L. (1991) *Protein Eng.* 4, 701–708.
- Edwards, S. L., and Poulos, T. L. (1990) *J. Biol. Chem.* 265, 2588–2595.
- Sundaramoorthy, M., Choudhury, K., Edwards, S. L., and Poulos, T. L. (1991) *J. Am. Chem. Soc.* 113, 7755–7757.
- Otwinowski, Z., and Minor, W. (1997) *Methods Enzymol.* 276, 307–326.
- Powell, H. R. (1999) *Acta Crystallogr. D10*, 1690–1695.
- Brunger, A. T., Adams, P. D., Clore, G. M., DeLano, W. L., Gros, P., Grosse-Kunstleve, R. W., Jiang, J.-S., Kuszewski, J., Nilges, M., Pannu, N. S., Read, R. J., Rice, L. M., Simonson, T., and Warren, G. L. (1998) *Acta Crystallogr. D54*, 905–921.
- Sheldrick, G. M., and Schneider, T. R. (1997) *Methods Enzymol.* 277, 319–343.
- Lee, F. S., Chu, Z. T., and Warshel, A. (1993) *J. Comput. Chem.* 14, 161–185.
- Jensen, G. M., Bunte, S. W., Warshel, A., and Goodin, D. B. (1998) *J. Phys. Chem. B* 102, 8221–8228.
- Poulos, T. L., and Kraut, J. (1980) *J. Biol. Chem.* 255, 8199–8205.
- Poulos, T. L., and Finzel, B. C. (1984) in *Peptide and Protein Reviews* (Mearn, M. T., Ed.) pp 115–171, Marcel Dekker, New York.
- Edwards, S. L., Poulos, T. L., and Kraut, J. (1984) *J. Biol. Chem.* 259, 12984–12988.
- Pelletier, H., and Kraut, J. (1992) *Science* 258, 1748–1755.
- Patterson, W. R., Poulos, T. L., and Goodin, D. B. (1995) *Biochemistry* 34, 4342–4345.
- Pappa, H., Patterson, W. H., and Poulos, T. L. (1996) *J. Biol. Inorg. Chem.* 1, 66.
- Purcell, W. L., and Erman, J. E. (1976) *J. Am. Chem. Soc.* 98, 7033–7077.
- Gouet, P., Jouve, H. M., Williams, P. A., Andersson, I., Andreoletti, P., Nussaume, L., and Hajdu, J. (1996) *Nat. Struct. Biol.* 3, 951–956.
- Hersleth, H. P., Dalhus, B., Gorbitz, C. H., and Andersson, K. K. (2002) *J. Biol. Inorg. Chem.* 7, 299–304.
- Berglund, G. I., Carlsson, G. H., Smith, A. T., Szoke, H., Henriksen, A., and Hajdu, J. (2002) *Nature* 417, 463–468.
- Chance, B., Powers, L., Ching, Y., Poulos, T., Schonbaum, G. R., Yamazaki, I., and Paul, K. G. (1984) *Arch. Biochem. Biophys.* 235, 596–611.
- Penner-Hahn, J., McMurry, T., Renner, M., Latos-Grazynsky, L., Eble, K. S., Davis, I. M., Balch, A. L., Groves, J. T., and Dawson, H. K. (1986) *J. Biol. Chem.* 261, 12761–12764.
- Reczek, C. M., Sitter, A. J., and Termer, J. (1989) *J. Mol. Struct.* 214, 27–41.
- Hashimoto, S., Teraoka, J., Inubushi, T., Yonetani, T., and Kitagawa, T. (1986) *J. Biol. Chem.* 261, 11110–11118.
- Sitter, A. J., Reczek, C. M., and Termer, J. (1985) *J. Biol. Chem.* 260, 7515–7522.
- Makino, R., Uno, T., Nishimura, Y., Iizuka, T., Tsuboi, M., and Ishimura, Y. (1986) *J. Biol. Chem.* 261, 8376–8382.
- Lang, G., Spartalian, K., and Yonetani, T. (1976) *Biochim. Biophys. Acta* 451, 250–258.
- Groves, J. T., Quinn, R., McMurray, T. J., Nakamura, M., Lang, G., and Boso, B. (1985) *J. Am. Chem. Soc.* 107, 354–360.
- Schonbaum, G. R., and Lo, S. (1972) *J. Biol. Chem.* 247, 3353–3360.
- Hirst, J., and Goodin, D. B. (2000) *J. Biol. Chem.* 275, 8582–8591.
- Li, H., Raman, C. S., Martasek, P., Masters, B. S., and Poulos, T. L. (2001) *Biochemistry* 40, 5399–5406.